Hydration of Portland cement accelerated by C-S-H seeds at different temperatures

Herman Camilo Pedrosa, Oscar Mendoza Reales, Victória Dias Reis, Maria das Dores Paiva, Eduardo Moraes Rego Fairbairn

[a] *Programa de Engenharia da Nanotecnologia PENt/COPPE, Universidade Federal do Rio de Janeiro, Brazil*
[b] *Programa de Engenharia Civil PEC/COPPE, Universidade Federal do Rio de Janeiro, Brazil*

A B S T R A C T

C-S-H seeds have potential application as accelerators in oil well cementing pastes. Typical oil well conditions present elevated temperatures; nevertheless, is not clear how such temperatures affect the nucleation process induced by these seeds. In this work, class G cement pastes were blended with up to 5.0% of C-S-H seeds and cured at 25, 40 and 60 °C. Hydration kinetics results showed that the nucleation effect from C-S-H seeds ac-celerated the reaction by decreasing the apparent activation energy of pastes. This acceleration was more ef-fective at lower temperatures. Nano-mechanical results showed that the main phases obtained from the hy-dration of cement paste blended with C-S-H seeds are capillary porous material and low density C-S-H. It was concluded that this higher amount of loosely packed hydrates is consequence of an increase in the number precipitation spots, and that their packing density depends on the curing temperature, and amount of C-S-H seeds used.

1. Introduction

Due to their high specific surface area, nanoparticles are capable of accelerating the kinetics of cement hydration by stimulating the nucleation and precipitation process of calcium silicate hydrate (C-S-H) as agglomerates during the initial hours of reaction [1,2]. This acceleration leads to a densification of the matrix by filling faster the space between cement grains with hydrated phases; thus, accelerating compressive strength development and reducing capillary porosity [1,3–5].

It is known the mechanical behavior of C-S-H presents nanogranular nature, meaning that particle-to-particle contact within the agglomerates has a greater influence over its mechanical response than the intrinsic properties of the phase [6]. Nanoindentation experiments have found that different packing densities lead to different elastic modulus, identifying at least three types of C-S-H, low density (LD), high density (HD) and ultra-high density (UHD) [7]. It is expected the precipitation process has a great influence over the spatial organization of C-S-H particles, which leads to the different packing densities agglomerates [6].

C-S-H seeds have been successfully used as nucleation spots to accelerate the hydration reaction of cement [4], finding shorter induction periods and higher heat flow values for C_3S in isothermal calorimetry results. It has been found that the magnitude of the accelerating effects depends on the amount of C-S-H seeds blended in the cement matrix, having a minimum amount of seeds necessary for the nucleation to become significant, and a maximum threshold above which more seeds do not result in further acceleration [4,8,9].

The thermal stability of the different C-S-H types has been studied in order to understand the behavior of Portland cement based matrices exposed to high temperatures. It is now clear that C-S-H presents different phase transitions [5] and decomposition mechanisms [10] at high temperature. Nevertheless, little attention has been given to the properties of C-S-H obtained from the hydration of pastes blended with C-S-H seeds at elevated temperatures. This scenario corresponds to oil well cementing applications, where the cementing paste can be exposed to temperatures over to 150 °C during the first hours of hydration in high-pressure high-temperature (HPHT) wells. The use of C-S-H seeds is interesting for oil well cementing since it has the potential of not only accelerating the hydration reaction, but also increasing the early age strength of the paste, which translates in a more efficient cementing process.

Since the hydration of cement is temperature-dependent and follows an Arrhenius equation [11,12], and since it is expected that the different packing densities of C-S-H depend heavily on the nucleation and

Table 1
Nomenclature, mass proportioning and testing temperatures of the studied pastes. (m.c.: mass of cement).

Paste	w/c	Cement (%)	C-S-H seeds (% m.c.)	Xanthan gum (% m.c.)	Temperature (°C)
REFEF	0.44	100	0	0.05	25, 40, 60
0.5% C-S-H seeds		100	0.5		
2.0% C-S-H seeds		100	2.0		
5.0% C-S-H seeds		100	5.0		

Table 2
Physical and chemical characteristics obtained for C-S-H seeds. (d_{10}, d_{50} and d_{90}: intercepts for 10%, 50% and 90% of the cumulative volume curve).

Particle size	(nm)
d_{10}	12.4
d_{50}	21.4
d_{90}	52.3
Specific surface area (m^2/g)	289

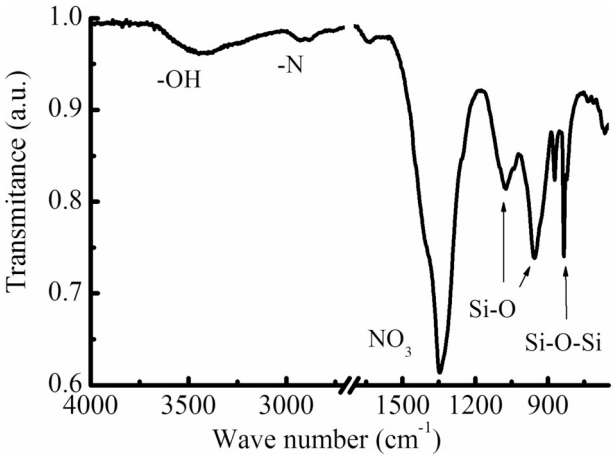

Fig. 1. FTIR transmittance spectra obtained for freeze-dried C-S-H seeds. (a.u.: arbitrary units).

precipitation process [6], it becomes interesting to study the C-S-H formed from the nucleation effect of C-S-H seeds and if its properties are temperature-dependent. The goal of this study is to characterize the effect of C-S-H seeds over the hydration kinetics and nano-mechanical properties of an oil well cementing paste cured at different temperatures.

2. Experimental procedures

2.1. Materials

The materials used in this study were class G Portland cement compliant with API 10A/ISO 10426-1 specification, a commercial aqueous suspension of C-S-H seeds commercial brand Master X-seed 100 produced by BASF Chemicals, and xanthan gum as a stabilizing agent of the paste to avoid water exudation and vertical gradient of solids.

2.2. Materials characterization

Characterization of the C-S-H seeds aqueous dispersion was performed through particle size distribution, Fourier-Transform Infrared (FTIR) spectroscopy, and Transmission Electron Microscopy (TEM). Particle size distribution was determined by laser diffraction using water as dispersing medium in a Mastersizer 3000 instrument from Malvern; this result was used to estimate the specific surface area of the seeds by assuming spherical individual particles. Water was removed from the suspension by freeze-drying in order to perform FTIR testing. FTIR was performed from 650 to 4000 cm^{-1} using an attenuated total reflectance (ATR) accessory in transmittance mode using a 6700 Nicolet instrument in order to identify the presence of dispersing agents. TEM imaging was performed by dispersing an aliquot of the C-S-H seeds aqueous dispersion in isopropanol using an ultrasonic bath for 30 min. A drop of this suspension was deposited on a carbon-coated TEM grid and dried at room temperature. Bright field images were acquired in a FEI 200 transmission microscope from TECNAI equipped with a Tungsten probe and operated at 80 kV. Imaging was carried out in magnifications between 80.000 and 120.00×.

2.3. Sample proportioning

Cement pastes were prepared with a fixed water-to-cement ratio (w/c) of 0.44 and 0.05% of xanthan gum as stabilizing agent. The w/c value was adopted from the API 10B recommended practice for testing well cements. Xanthan gum was added in an amount enough to obtain 0% static sedimentation, also following API 10B recommended practice. C-S-H seeds were added in three percentages (0.5%, 2.0% and 5.0%) by mass of cement. Hydration kinetics and nano-mechanical testing were performed in these pastes at three different temperatures (25, 40 and 60 °C). The maximum curing temperature was chosen to represent the typical bottom-hole temperature in Brazilian oil wells, and to avoid thermal decompositions or phase transitions during the experiments. A summary of the studied pastes is presented in Table 1.

2.4. Hydration kinetics testing

The influence of the C-S-H seeds over the hydration kinetics of cement paste was studied using two techniques: isothermal calorimetry to characterize the heat release evolution, and ultrasonic pulse velocity to characterize the setting and hardening of the pastes. Isothermal calorimetry testing was performed according to the BS EN 196-11:2018 standard using water as reference material in a TAM Air isothermal calorimeter from TA Instruments. Heat flow and heat results were acquired continuously for 100 h at each testing temperature. The apparent activation energy (E_a) of each formulation was obtained from heat flow results at the same hydration degree (α) in three temperatures using the linear method. This method is based on a linearization of the Arrhenius equation, ($k = Ae^{-Ea/RT}$), where k is the temperature-

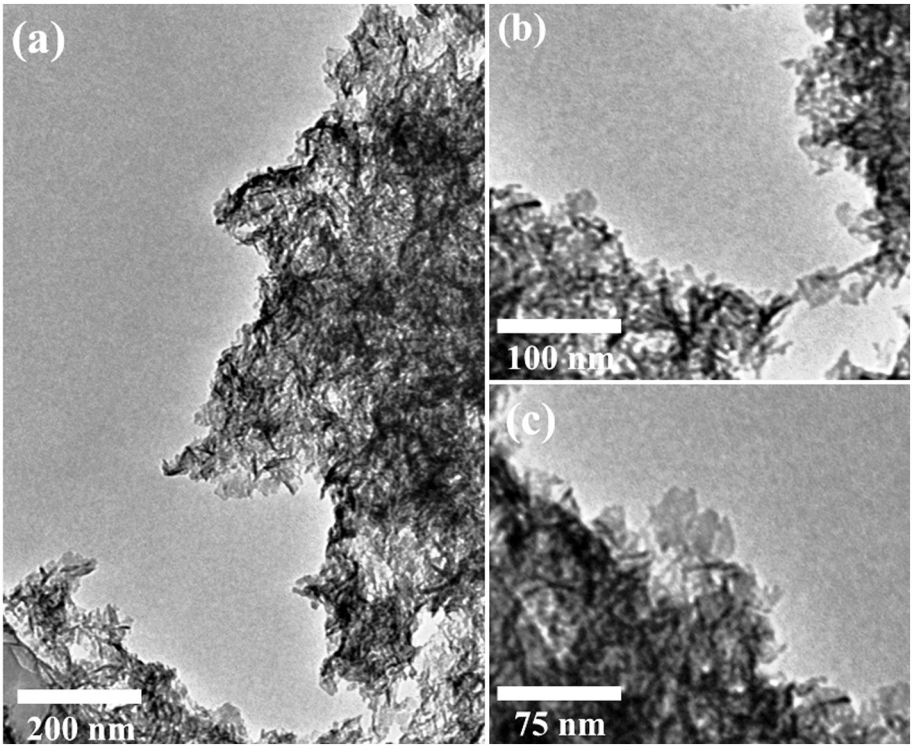

Fig. 2. TEM imaging of C-S-H seeds. (a) C-S-H seeds agglomerate, and (b), (c) detail on individual seeds.

dependent rate of heat generation, A is the pre-exponential factor, T is the temperature, and R is the universal gas constant (8.3144 J/K·mol) [13].

Setting and hardening of the pastes was studied using an ultrasonic cement analyzer Twin Cell UCA from Chandler Engineering. Pastes were mixed in a 600 ml constant speed mixer following the procedure in API 10B recommended practice and placed in the equipment at the testing temperatures with no pressure applied. Ultrasonic wave velocities through a mass of paste were acquired continuously for 170 h. The kinetics of the setting process was characterized through the percolation threshold, which was defined as the time corresponding to the first inflexion point of the wave velocity versus time curve, where the paste stops behaving like a fluid and starts behaving as a solid [14]. The kinetics of the hardening process (strength gain) was characterized through the evolution over time of the wave velocity, which is proportional to the modulus of elasticity and compressive strength of the material [15].

2.5. Nano-mechanical testing

The influence of C-S-H seeds on the mechanical properties of the C-S-H precipitated during cement hydration at different temperatures was studied by statistical nanoindentation. Portions of the samples mixed for ultrasonic testing were cured for 28 days in watertight containers at each testing temperature. After curing, pastes were mounted in epoxy resin and sanded in an automatic grinder using a rotation velocity of 150 rpm and 125, 70, 40, 15, 9 and 6 μm polishing discs. Finally, samples were polished using cloths with 3 and 1 μm diamond particles. Each sample was sanded or polished for 20 min in each disc, using isopropyl alcohol as refrigerant media. Nanoindentation tests were carried out using a using a G200-MTS system nanoindenter equipped with a Berkovich tip and fused silica as reference material. One test, consisting of a 10 × 10 indentation grid, was performed on each sample. Indentations were evenly spaced each 15 μm in both directions; this spacing was determined in order to guarantee an adequate coverage of different hydrated phases [6]. The maximum load used in each indent was 2 mN, applied in 10 s (loading), held for 5 s, and released in 5 s (unloading) [16]. The elastic modulus at each indented point was determined from the unloading portion of the curve following the equations proposed by Oliver and Pharr [17]. Individual phases were identified through their modulus of elasticity using deconvolution. Relative and cumulative frequency counts were constructed for each indentation grid. Five Gaussian probability distribution functions (PDF) were adjusted to each experimental cumulative distribution function (CDF), each PDF corresponding to a mechanically distinct phase [18]. For this purpose, a simple search algorithm can be applied, using the quadratic error between experimental and theoretical PDF as objective function and proportions of each phase as linear constraints.

3. Results and discussion

3.1. Materials characterization

Characterization of the C-S-H seeds is presented in Table 2 and Figs. 1 and 2. Particle size and specific surface area results confirmed the nanometric nature of the seeds. FTIR results showed bands associated with vibrational modes of Si—O, Si-O-Si and –OH bonds, typical of C-S-H [19]. Additional NO_3 and —N vibration modes were identified, which can be associated with the probable use of a nitrate based compound as dispersing agent for the C-S-H seeds in the aqueous media. TEM images showed C-S-H seeds agglomerates (Fig. 2(a)) consequence of the drying procedure for sample preparation. Nevertheless, individual particles of sizes compatible with those found in particle size distribution experiments could be identified (Fig. 2(b) and (c)). C-S-H

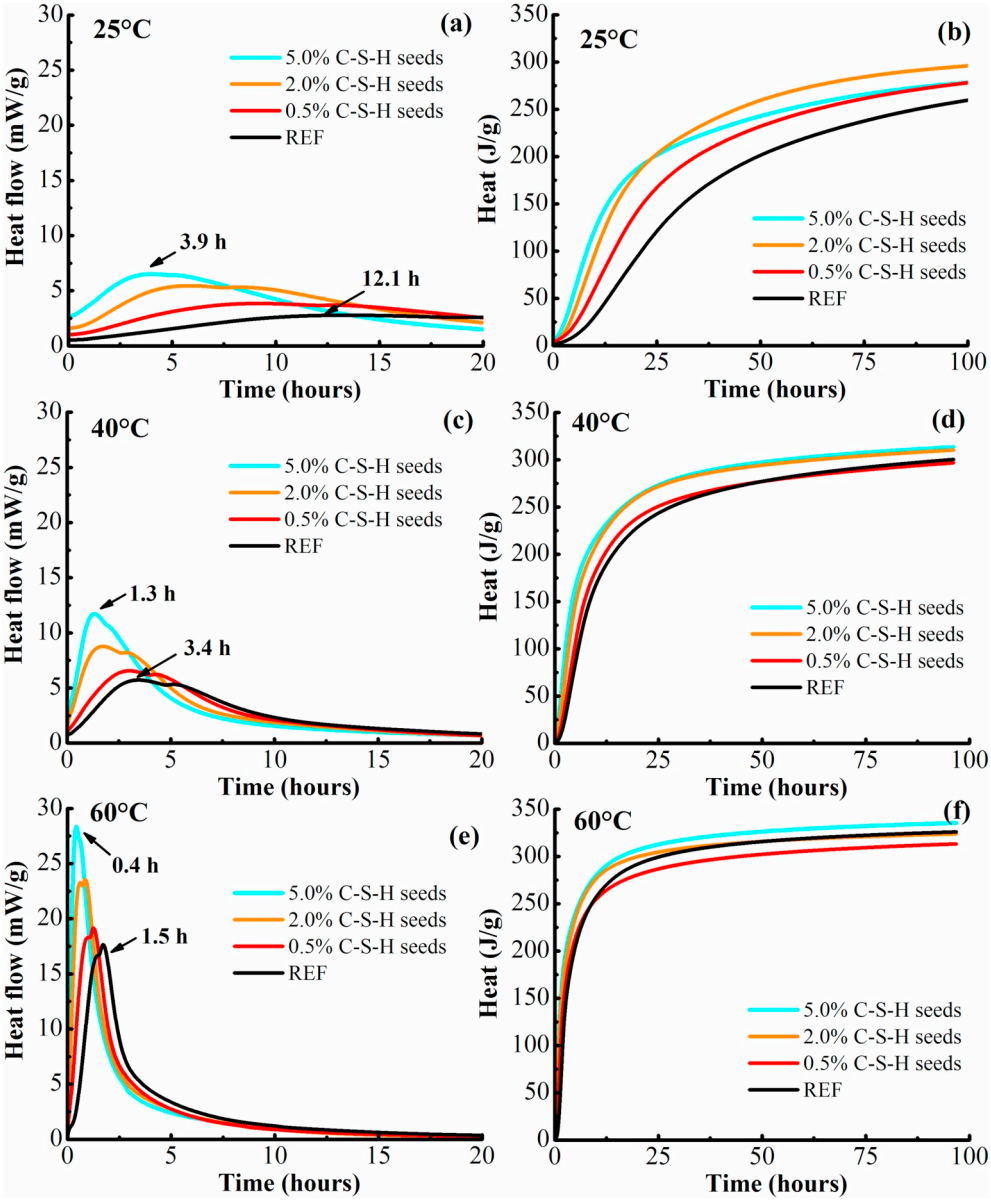

Fig. 3. Heat flow and cumulative heat results obtained from isothermal calorimetry testing for all pastes blended with C-S-H seeds and cured at (a–b) 25 °C, (c–d) 40 °C and (e–f) 60 °C.

seeds were found to have foil-like morphology, compatible with the morphologies previously reported in the literature [20,21], especially with those from C-S-H obtained by mechanochemical treatments and silica-lime reactions [22].

3.2. Hydration kinetics

The effect of C-S-H seeds over the hydration kinetics of cement was studied by isothermal calorimetry. Heat flow results normalized by mass of cement for all studied pastes are presented in Fig. 3(a), (c) and (e). It was found, as expected, that the hydration reaction was accelerated both by temperature and by the presence of C-S-H seeds. This acceleration was identified as a shift to the left of the main hydration peak, which corresponds to the C-S-H precipitation [23]. Within each temperature, acceleration was found to be proportional to the amount of C-S-H seeds in the paste, consequence of the nucleation effect of C-S-H seeds [24]. Taking as reference point the maximum value of the main heat flow peak, it can be seen that 5.0% C-S-H seeds were able to decrease the time when this maximum appeared by 4.0 times at 25 °C, 2.6 times at 40 °C and 3.7 times at 60 °C.

Heat results by mass of cement for all studied pastes are presented in Fig. 3(b), (d) and (f). When comparing to the reference samples, it was found that the acceleration effect induced by the nucleation of C-S-H seeds seems to be restricted to the first hours of hydration, especially for higher temperatures and higher C-S-H seeds concentrations. At 25 °C, 0.5% and 2.0% C-S-H seeds were able to increase significantly the total heat released after 100 h of testing, while the 5.0% C-S-H seeds sample showed a lower efficiency from the 24th hour ahead. This behavior is

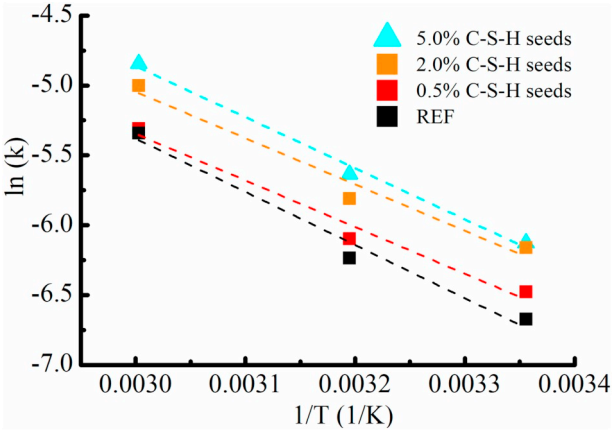

Fig. 4. Natural logarithm of reaction rate versus the inverse of temperature obtained for all pastes blended with C-S-H seeds. (Dotted lines correspond to the fitting of a linearized Arrhenius equation).

Table 3
Apparent activation energy (E_a) results and correlation coefficients (r^2) obtained from the fitting of a linearized Arrhenius equation at $\alpha = 0.5$ for all pastes blended with C-S-H seeds.

Sample	E_a (kJ/mol)	r^2
REF	31.64	0.979
0.5% C-S-H seeds	27.76	0.978
2.0% C-S-H seeds	27.57	0.970
5.0% C-S-H seeds	30.39	0.993

consistent with a heterogeneous nucleation mechanism, which depends on the available number of nuclei and surface area [25]. It should be noticed that some literature reports have proposed that the nucleation of C-S-H is a two-step nonclassical nucleation process, but that this mechanism might not be applicable to real matrices [26].

At 40 °C and 60 °C, the total heat released after 100 h of testing does not seem to be significantly influenced by the presence of C-S-H seeds, having some pastes releasing slightly lower amounts of heat than the reference paste. This indicates that at higher temperatures, where all the reactions occur more rapidly, the point where the nucleation of C-S-H seeds ceases and becomes negligible for total heat released is reached faster.

To better understand the effect of C-S-H seeds on the hydration reaction of cement, isolated from the effect of temperature, E_a was estimated for each formulation by fitting a linearized Arrhenius equation to the natural logarithm of the heat flow corresponding to a hydration degree of $\alpha = 0.5$ at each testing temperature. The hydration degree was defined as $\alpha = H_{(i)}/H_u$, where $H_{(i)}$ is the cumulative heat released by the hydration reaction at a given time, and $H_u = 358.96$ J/g is the total amount of heat released by the reference sample after 28 days of continuous testing in the isothermal calorimeter. The obtained results are presented in Fig. 4 and Table 3. These values agree in magnitude with several literature reports for C_3S [27,28] and cement paste blended with nanoparticles [13], which are characteristic of processes controlled by rates of chemical reaction. It was found that the nucleation effect of C-S-H seeds decreases E_a, i.e. decreases the minimum amount of energy required for the mixture to undergo chemical reaction [11]. Nevertheless, this effect was found to be less significant with the increasing content of C-S-H seeds in the paste, being 2.0% the most efficient amount of C-S-H seeds for this matter. The source of this loss of efficiency should be further studied, but it might be related with a less uniform dispersion of a high amount of seeds in the matrix.

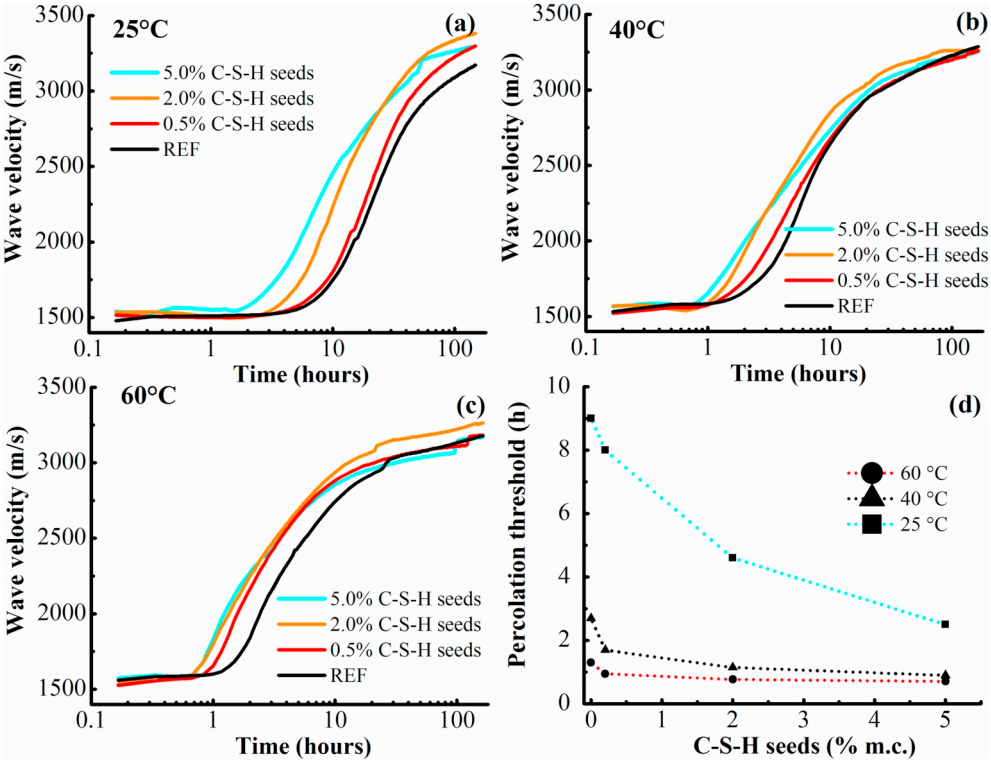

Fig. 5. Ultrasonic pulse velocity results obtained for all pastes blended with C-S-H seeds and cured at (a) 25 °C, (b) 40 °C, (c) 60 °C, and (d) percolation threshold results.

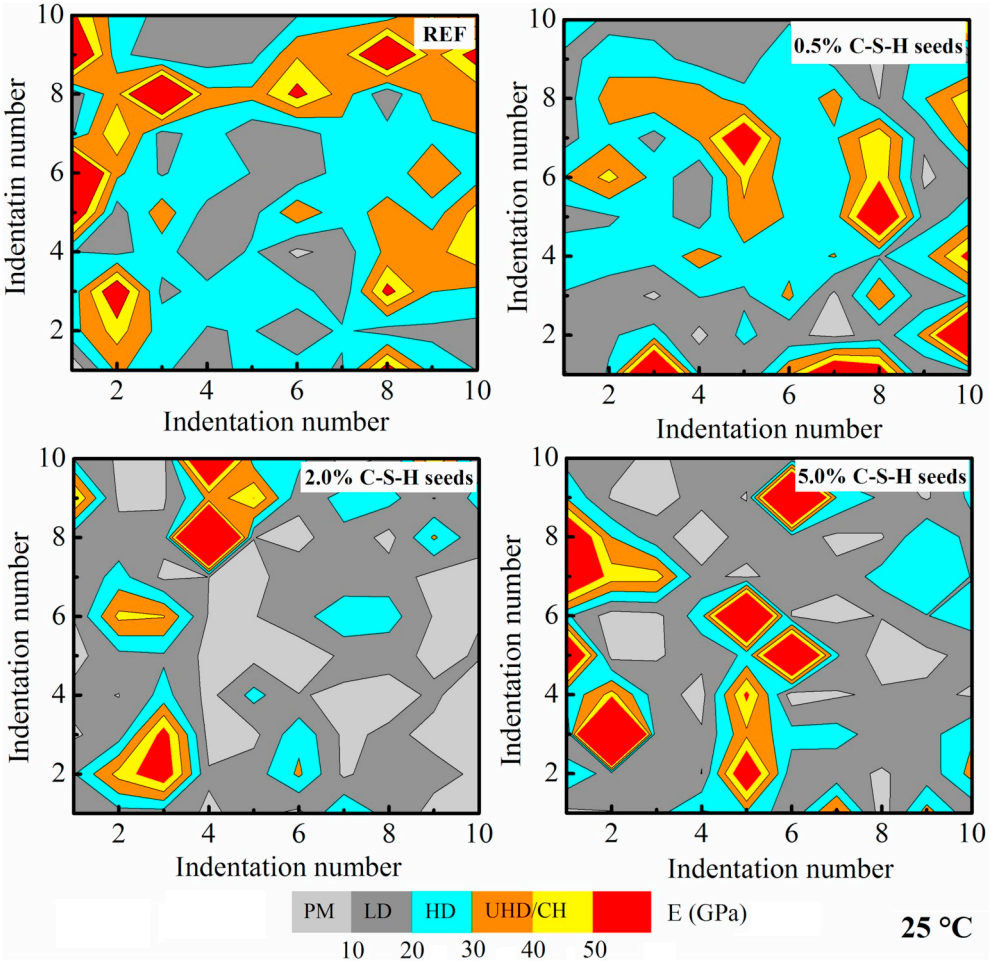

Fig. 6. Elastic modulus maps of the indented 150 × 150 μm^2 areas obtained from all pastes blended with C-S-H seeds and cured at 25 °C. (PM: porous material, LD; low density C-S-H, HD: high density C-S-H, UHD: ultrahigh density C-S-H, CH: calcium hydroxide).

Nevertheless, it should be noted that some authors have proposed a two-step nonclassical nucleation process for C-S-H, where C-S-H would not serve as substrate for heterogeneous nucleation; thus, expecting that C-S-H will precipitate around the anhydrous grains even at high dosages of C-S-H seeds [26,29].

The effect of C-S-H seeds over the hydration kinetics was also studied through the setting and hardening processes. Ultrasonic pulse velocity and percolation threshold results for all studied pastes are presented in Fig. 5. Similarly to the heat release results, it was found that the percolation threshold of pastes decreased by the presence of C-S-H seeds, showing an acceleration of setting time. Again, C-S-H seeds presented a more pronounced effect at 25 °C, decreasing the time for the percolation threshold by up to 3.6 times for the 5.0% C-S-H seeds paste. For the same paste, at 40 °C, the time for the percolation threshold was decreased by 3.0 times, and at 60 °C it was decreased by 1.8 times. This indicates that C-S-H seeds are efficient accelerators for setting time at low temperatures, and that their effect becomes less efficient with the increase in temperature.

Regarding strength development, wave velocity results presented a similar trend to the one obtained from heat release results. It was found that immediately after the percolation threshold, the addition of C-S-H seeds caused the development of higher wave velocity values in shorter times. This is equivalent to a more rapid compressive strength development, and was found to be true for all temperatures tested. Nevertheless, after 170 h of curing, only the samples cured at 25 °C maintained a significant increase in wave velocity, being 2.0% the most efficient amount of C-S-H seeds in doing so. For the pastes cured at 40 °C and 60 °C, the increase in wave velocity became negligible after 170 h. This behavior is consistent with acceleration by nucleation, which enhances the hydration reaction and strength development at early ages, but due to the lack of pozzolanic activity, no additional strength is gained at later ages [24].

3.3. Nano-mechanical testing

Contour maps were plotted for each 10 × 10 indentation grid. E values for points where an indentation could not be performed were obtained by averaging the E values from all the direct neighboring indentations. The obtained maps are presented in Figs. 6, 8 and 10. Frequency counts for each indentation grid and the Gaussian PDFs obtained from deconvolution are presented in Figs. 7, 9 and 11. For the interpretation of the contour maps and frequency counts a range of E values was assigned to a specific phase using values obtained from the literature as follows: Capillary porous material (PM) from 0 to 10.0 GPa, Low Density C-S-H (LD) from 10.0 to 20.0 GPa, High Density C-S-H (HD) from 20.0 to 30 GPa, Ultra High Density C-S-H and Calcium

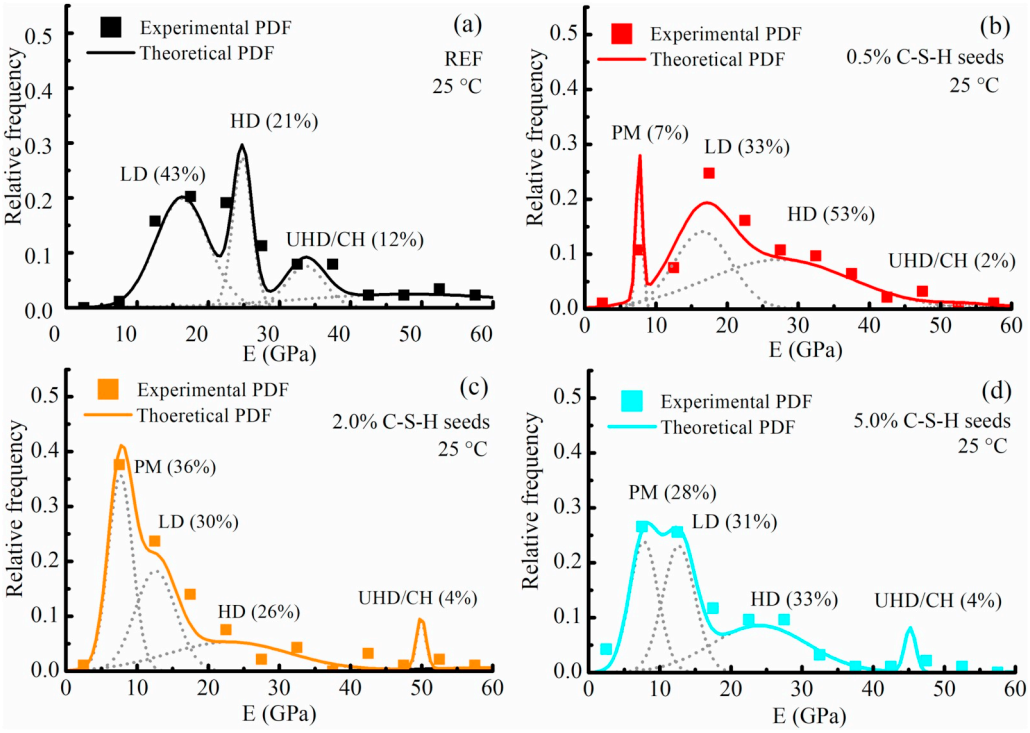

Fig. 7. Deconvolution results of the E frequency counts obtained from all pastes blended with C-S-H seeds and cured at 25 °C. (PDF: probability distribution function, M: porous material, LD: low density C-S-H, HD: high density C-S-H, UHD: ultrahigh density C-S-H, CH: calcium hydroxide).

Hydroxide (UHD/CH) from 30.0 to 50.0 GPa. Higher values were attributed to carbonated material and non-hydrated clinker [7,16,30–32].

Frequency counts and Gaussian PFDs for all samples cured at 25 °C are presented in Fig. 7. It was found that the main phase present in the reference paste after 28 days of curing was LD C-S-H, followed by HD C-S-H and UHD C-S-H/CH. No significant amount of capillary porous material was identified at this stage. It was also found that the presence of C-S-H seeds increased the amount of PM and LD C-S-H, at the expense of HD-C-S-H and UHD C-S-H/CH. Similarly to the other experiments studied in this work, 2.0% C-S-H seeds was the amount of nanoparticles that presented the highest effect on the paste. The contour maps of the same samples (Fig. 6) showed that PM and LD C-S-H grew around nuclei of non-hydrated clinker grains, in the space probably occupied initially by the mixing water.

Frequency counts and Gaussian PDFs for all samples cured at 40 °C and 60 °C (Figs. 9 and 11) showed a similar effect towards lower density phases when C-S-H seeds were blended to the paste. At these temperatures the main phases found in the reference paste were HD C-S-H and UHD C-S-H/CH, followed by small amounts of LD C-S-H. This agrees with previous literature reports showing that higher curing temperatures favor the formation of high-density phases [7]. The presence of C-S-H seeds increased the number of precipitation spots, stimulating the formation of LD C-S-H which would later densify to form HD C-S-H and UHD C-S-H/CH. At these temperatures almost no PM was identified as result of nucleation, which is also consistent with a more advanced hydration reaction. Contour maps of the same samples (Figs. 8 and 10) showed UHD C-S-H/CH grew preferentially around the non-hydrated clinker grains, while HD C-S-H grew more evenly distributed, leaving some isolated nuclei of LD C-S-H.

4. Final discussion

As expected, C-S-H seeds were able to accelerate the main heat release peak of hydration (C-S-H precipitation) and consequently reduce the setting time of cement paste. This behavior has been associated to nucleation effect of the seeds [24], which decreases the apparent activation energy of the paste, as was demonstrated in this work. The accelerating effects identified were found to be consistent with a heterogeneous nucleation process, which is very efficient during the first hours, but as time progresses it loses efficiency [25]. Additionally, at higher temperatures where all the reactions occur more rapidly, the point where the nucleation effect of C-S-H seeds ceases and becomes negligible was reached faster.

Nanoindentation results showed a higher formation of low density phases due to the increase of precipitation spots induced by the C-S-H seeds, which then densify with the hydration degree. It has been previously proposed C-S-H from regular cement hydration grows loosely packed in needle like morphologies [33] and later densifies [34]. The statistical Nanoindentation results presented in this work suggest C-S-H growing from the nucleation of C-S-H seeds also grows loosely packed, starting as capillary porous material and LD C-S-H, and later becomes HD C-S-H and UHD C-S-H.

To better visualize the effects induced by C-S-H seeds, the hydration degree of each sample was computed both after 60 h and 28 days of hydration. The hydration degree after 60 h of hydration ($\alpha_{60\ hours}$) was defined as the total amount of heat released after 60 h of isothermal calorimetry testing ($H_{60\ hours}$), divided by H_u. The hydration degree after 28 days of hydration ($\alpha_{28\ days}$) was computed using the obtained E_a from the linearization of the Arrhenius equation, the isothermal calorimetry results, and a three-parameter exponential model to characterize the degree of hydration ($\alpha(t_e) = \alpha_u \cdot e^{-\left(\tau/t_e\right)^{\beta}}$), where α_u is the

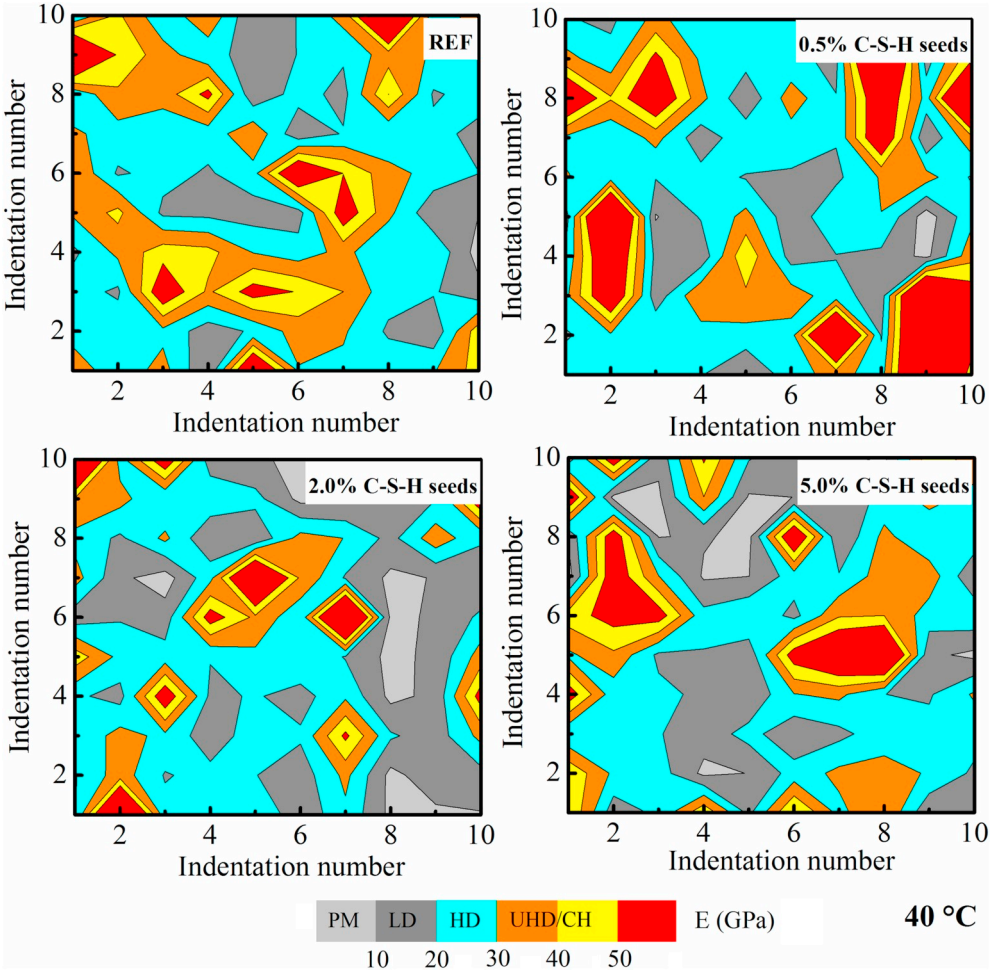

Fig. 8. Elastic modulus maps of the indented 150 × 150 μm^2 areas obtained from all pastes blended with C-S-H seeds and cured at 40 °C. (PM: porous material, LD; low density C-S-H, HD: high density C-S-H, UHD: ultrahigh density C-S-H, CH: calcium hydroxide).

maximum hydration degree and τ and β are hydration time and shape parameters, and t_e is the equivalent time [13]. For this purpose, the equivalent age formula was used, $\left(t_e = \int_{t_0}^{t} e^{\frac{E_a}{R}\left(\frac{1}{T_c}-\frac{1}{T_r}\right)} dt\right)$; where T_c is the temperature of the sample, T_r is the reference temperature (298 K), and t-t_0 is the curing time at the sample temperature [11,12]. Results are presented in Table 4. It can be seen that after 60 h of hydration, the hydration degree increases both with temperature and with the presence of C-S-H seeds up to 2.0%. This was expected, since cumulative heat release results showed that after 60 h the accelerating effect of C-S-H seeds is still significant and may lead to a more mature matrix. Whereas, after 28 days of hydration, almost all samples reached a similar hydration degree, with the exception of the highest amount of C-S-H seeds cured at 25 °C. This might partly explain the formation of less dense C-S-H; nevertheless, more experiments are required to establish a reliable correlation between packing density, hydration degree and amount of C-S-H seeds.

5. Conclusions

After verifying the accelerating effect of the C-S-H seeds over the hydration reaction of Portland cement paste, it was possible to gain additional insights on the mechanisms behind this acceleration and the effect of curing temperature over it. The evidence gathered in this work allows concluding the following:

- The nucleation effect of the C-S-H seeds accelerates hydration, decreasing the apparent activation energy of the pastes.
- C-S-H obtained from the nucleation of C-S-H seeds grows loosely packed as consequence of an increase in the number precipitation spots, and its packing density depends on the curing temperature and amount of C-S-H seeds used.
- The nucleation effect of C-S-H seeds becomes less efficient at higher temperatures, limiting its applicability in oil well cementing applications.

Declaration of competing interest

The authors declare that they have no known competing financial interests or personal relationships that could have appeared to influence the work reported in this paper.

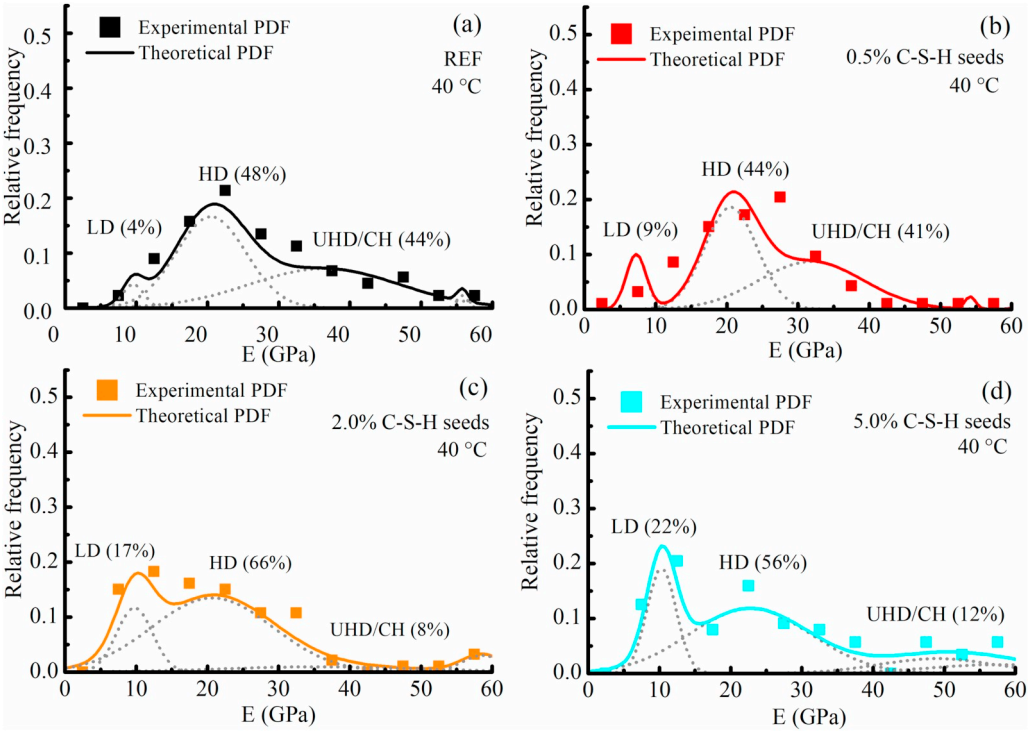

Fig. 9. Deconvolution results of the E frequency counts obtained from all pastes blended with C-S-H seeds and cured at 40 °C. (PDF: probability distribution function, M: porous material, LD: low density C-S-H, HD: high density C-S-H, UHD: ultrahigh density C-S-H, CH: calcium hydroxide).

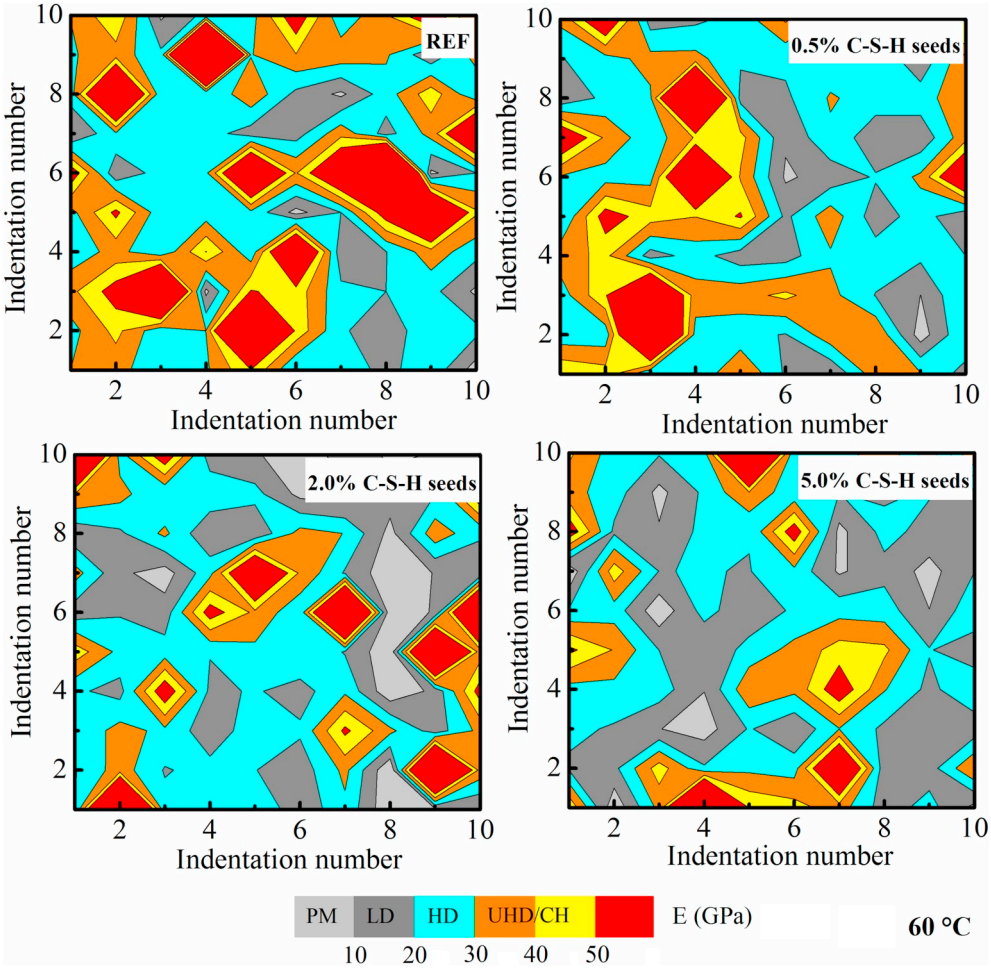

Fig. 10. Elastic modulus maps of the indented 150 × 150 μm^2 areas obtained from all pastes blended with C-S-H seeds and cured at 60 °C. (PM: porous material, LD; low density C-S-H, HD: high density C-S-H, UHD: ultrahigh density C-S-H, CH: calcium hydroxide).

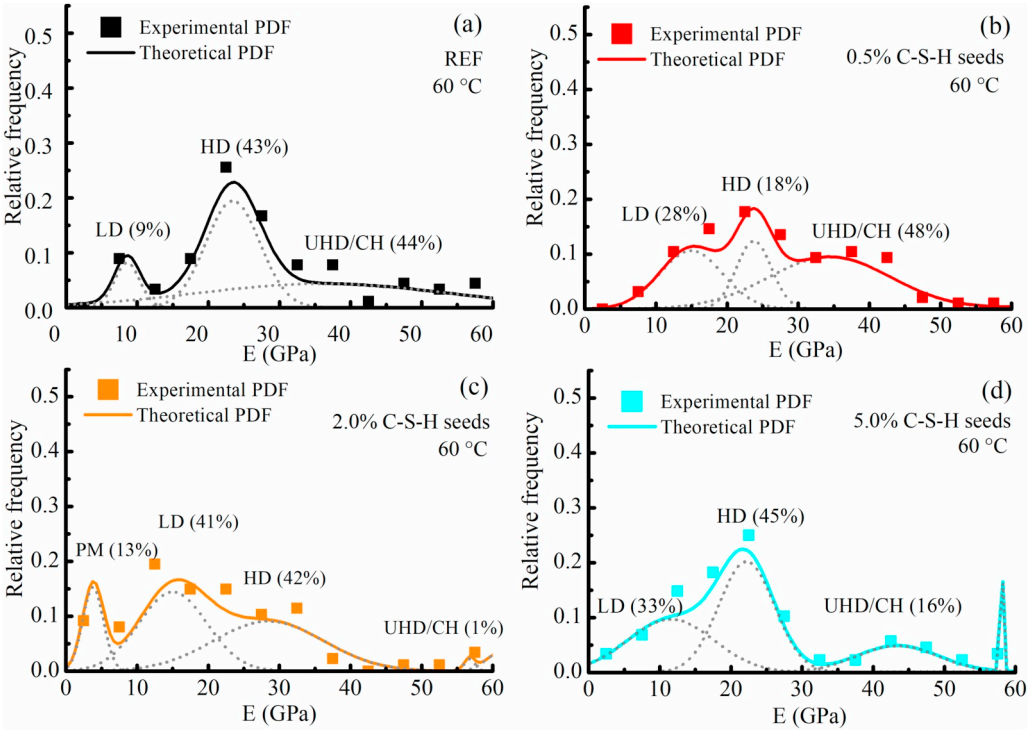

Fig. 11. Deconvolution results of the E frequency counts obtained from all pastes blended with C-S-H seeds and cured at 60 °C. (PDF: probability distribution function, M: porous material, LD: low density C-S-H, HD: high density C-S-H, UHD: ultrahigh density C-S-H, CH: calcium hydroxide).

Table 4
Hydration degree after 60 h ($\alpha_{60\ hours}$) and 28 days ($\alpha_{28\ days}$) for all pastes blended with C-S-H seeds.

Sample	$\alpha_{60\ hours}$			$\alpha_{28\ days}$		
	25 °C	40 °C	60 °C	25 °C	40 °C	60 °C
REF	0.74	0.83	0.91	0.93	0.91	0.95
0.5% C-S-H seeds	0.77	0.83	0.87	0.93	0.90	0.91
2.0% C-S-H seeds	0.83	0.86	0.90	0.94	0.92	0.93
5.0% C-S-H seeds	0.79	0.87	0.93	0.88	0.93	0.96

Acknowledgements

This study was financed in part by the Coordenação de Aperfeiçoamento de Pessoal de Nível Superior - Brasil (CAPES) - Finance Code 001.

References

[1] M. Bräu, L. Ma-Hock, C. Hesse, L. Nicoleau, V. Strauss, S. Treumann, K. Wiench, R. Landsiedel, W. Wohlleben, Nanostructured calcium silicate hydrate seeds accelerate concrete hardening: a combined assessment of benefits and risks, Arch. Toxicol. 86 (2012) 1077–1087, https://doi.org/10.1007/s00204-012-0839-x.
[2] L. Nicoleau, Accelerated growth of calcium silicate hydrates: experiments and simulations, Cem. Concr. Res. 41 (2011) 1339–1348, https://doi.org/10.1016/j.cemconres.2011.04.012.
[3] G. Land, D. Stephan, Controlling cement hydration with nanoparticles, Cem. Concr. Compos. 57 (2015) 64–67, https://doi.org/10.1016/j.cemconcomp.2014.12.003.
[4] G. Land, D. Stephan, Preparation and application of nanoscaled C-S-H as an accelerator for cement hydration, Nanotechnol. Constr, 2015, pp. 117–122, , https://doi.org/10.1007/978-3-319-17088-6.
[5] E. Tajuelo Rodriguez, K. Garbev, D. Merz, L. Black, I.G. Richardson, Thermal stability of C-S-H phases and applicability of Richardson and Groves' and Richardson C-(A)-S-H(I) models to synthetic C-S-H, Cem. Concr. Res. 93 (2017) 45–56, https://doi.org/10.1016/j.cemconres.2016.12.005.
[6] G. Constantinides, F.-J. Ulm, The nanogranular nature of C–S–H, J. Mech. Phys. Solids 55 (2007) 64–90, https://doi.org/10.1016/j.jmps.2006.06.003.
[7] M. Vandamme, F.-J. Ulm, P. Fonollosa, Nanogranular packing of C–S–H at substochiometric conditions, Cem. Concr. Res. 40 (2010) 14–26, https://doi.org/10.1016/j.cemconres.2009.09.017.
[8] V. Kanchanason, J. Plank, Role of pH on the structure, composition and morphology of C-S-H–PCE nanocomposites and their effect on early strength development of Portland cement, Cem. Concr. Res. 102 (2017) 90–98, https://doi.org/10.1016/j.cemconres.2017.09.002.
[9] V. Kanchanason, J. Plank, Effectiveness of a calcium silicate hydrate – polycarboxylate ether (C-S-H–PCE) nanocomposite on early strength development of fly ash cement, Constr. Build. Mater. 169 (2018) 20–27, https://doi.org/10.1016/j.conbuildmat.2018.01.053.
[10] M.J. DeJong, F.J. Ulm, The nanogranular behavior of C-S-H at elevated temperatures (up to 700 °C), Cem. Concr. Res. 37 (2007) 1–12, https://doi.org/10.1016/j.cemconres.2006.09.006.
[11] Q. Xu, J.M. Ruiz, J. Hu, K. Wang, R.O. Rasmussen, Modeling hydration properties and temperature developments of early-age concrete pavement using calorimetry tests, Thermochim. Acta 512 (2011) 76–85, https://doi.org/10.1016/j.tca.2010.09.003.
[12] Q. Xu, J. Hu, J.M. Ruiz, K. Wang, Z. Ge, Isothermal calorimetry tests and modeling of cement hydration parameters, Thermochim. Acta 499 (2010) 91–99, https://doi.org/10.1016/j.tca.2009.11.007.
[13] A.R. Jayapalan, M.L. Jue, K.E. Kurtis, Nanoparticles and apparent activation energy of Portland cement, J. Am. Ceram. Soc. 97 (2014) 1534–1542, https://doi.org/10.1111/jace.12878.
[14] G. Sant, M. Dehadrai, D. Bentz, P. Lura, C.F. Ferraris, J.W. Bullard, J. Weiss, Detecting the fluid-to-solid transition in cement pastes, Concr. Int. 236 (2009) 53–58.
[15] J. Zhang, L. Qin, Z. Li, Hydration monitoring of cement-based materials with resistivity and ultrasonic methods, Mater. Struct. 42 (2009) 15–24, https://doi.org/10.1617/s11527-008-9363-0.
[16] O. Mendoza, C. Giraldo, S.S. Camargo, J.I. Tobón, Structural and nano-mechanical properties of Calcium Silicate Hydrate (C-S-H) formed from alite hydration in the presence of sodium and potassium hydroxide, Cem. Concr. Res. 74 (2015) 88–94, https://doi.org/10.1016/j.cemconres.2015.04.006.
[17] W.C. Oliver, G.M. Pharr, An improved technique for determining hardness and elastic modulus using load and displacement sensing indentation experiments, Mater. Res. 7 (1992) 1564–1583.
[18] F.J. Ulm, M. Vandamme, C. Bobko, J. Alberto Ortega, K. Tai, C. Ortiz, Statistical indentation techniques for hydrated nanocomposites: concrete, bone, and shale, J. Am. Ceram. Soc. 90 (2007) 2677–2692, https://doi.org/10.1111/j.1551-2916.2007.02012.x.
[19] I. García Lodeiro, D.E. Macphee, A. Palomo, A. Fernández-Jiménez, Effect of alkalis on fresh C–S–H gels. FTIR analysis, Cem. Concr. Res. 39 (2009) 147–153, https://doi.org/10.1016/j.cemconres.2009.01.003.
[20] I. Richardson, Tobermorite/jennite- and tobermorite/calcium hydroxide-based models for the structure of C-S-H: applicability to hardened pastes of tricalcium silicate, ?-dicalcium silicate, Portland cement, and blends of Portland cement with blast-furnace slag, metakaol, Cem. Concr. Res. 34 (2004) 1733–1777, https://doi.org/10.1016/j.cemconres.2004.05.034.

[21] I.G. Richardson, The nature of C-S-H in hardened cements, Cem. Concr. Res. 29 (1999) 1131–1147.
[22] E. Tajuelo Rodriguez, I.G. Richardson, L. Black, E. Boehm-Courjault, A. Nonat, J. Skibsted, Composition, silicate anion structure and morphology of calcium silicate hydrates (C-S-H) synthesised by silica-lime reaction and by controlled hydration of tricalcium silicate (C3S), Adv. Appl. Ceram. 114 (2015) 362–371, https://doi.org/10.1179/1743676115y.0000000038.
[23] K.L. Scrivener, P. Juilland, P.J.M. Monteiro, Advances in understanding hydration of portland cement, Cem. Concr. Res. 78 (2015) 38–56, https://doi.org/10.1016/j.cemconres.2015.05.025.
[24] E. John, T. Matschei, D. Stephan, Nucleation seeding with calcium silicate hydrate – a review, Cem. Concr. Res. 113 (2018) 74–85, https://doi.org/10.1016/j.cemconres.2018.07.003.
[25] S. Garrault-Gauffinet, A. Nonat, Experimental investigation of calcium silicate hydrate (C-S-H) nucleation, J. Cryst. Growth 200 (1999) 565–574, https://doi.org/10.1016/S0022-0248(99)00051-2.
[26] N. Krautwurst, L. Nicoleau, M. Dietzsch, I. Lieberwirth, C. Labbez, A. Fernandez-Martinez, A.E.S. Van Driessche, B. Barton, S. Leukel, W. Tremel, Two-step nucleation process of calcium silicate hydrate, the nanobrick of cement, Chem. Mater. 30 (2018) 2895–2904, https://doi.org/10.1021/acs.chemmater.7b04245.
[27] J.J. Thomas, H.M. Jennings, Effects of D2O and mixing on the early hydration kinetics of tricalcium silicate, Chem. Mater. 11 (1999) 1907–1914, https://doi.org/10.1021/cm9900857.
[28] P. Juilland, E. Gallucci, Morpho-topological investigation of the mechanisms and kinetic regimes of alite dissolution, Cem. Concr. Res. 76 (2015) 180–191, https://doi.org/10.1016/j.cemconres.2015.06.001.
[29] P. Juilland, L. Nicoleau, R.S. Arvidson, E. Gallucci, Advances in dissolution understanding and their implications for cement hydration, RILEM Tech. Lett. 2 (2017) 90–98, https://doi.org/10.21809/rilemtechlett.2017.47.
[30] G. Constantinides, F.-J. Ulm, The effect of two types of C-S-H on the elasticity of cement-based materials: results from nanoindentation and micromechanical modeling, Cem. Concr. Res. 34 (2004) 67–80, https://doi.org/10.1016/S0008-8846(03)00230-8.
[31] J. Han, G. Pan, W. Sun, Elastic modulus change investigation of cement paste before and after carbonation using nanoindentation technique, Procedia Eng. 27 (2012) 341–347, https://doi.org/10.1016/j.proeng.2011.12.461.
[32] G. Constantinides, F. Ulm, K. Van Vliet, On the use of nanoindentation for cementitious materials, Mater. Struct. 36 (2003) 191–196.
[33] A. Ouzia, K. Scrivener, The needle model: a new model for the main hydration peak of alite, Cem. Concr. Res. 115 (2019) 339–360, https://doi.org/10.1016/j.cemconres.2018.08.005.
[34] S. Bishnoi, K.L. Scrivener, Studying nucleation and growth kinetics of alite hydration using μic, Cem. Concr. Res. 39 (2009) 849–860, https://doi.org/10.1016/j.cemconres.2009.07.004.